Available online www.jsaer.com

***Journal of Scientific and Engineering Research*, 2019, 6(5):89-94**

Research Article

ISSN: 2394-2630
CODEN(USA): JSERBR

A Numerical Integration Scheme for the Growth of a Fission Yeast Cell Based on the Self-Similarity Growth Principle

Najib A. Kasti

Beirut Arab University
e-mail: najib01@idm.net.lb

Abstract In a previous publication, the growth of the old end of the fission yeast cell was modeled using the self-similarity growth principle. This was justified since the shape of the old end and the width of the cell were almost constant with time. The geometry of the cell was assumed to be made of a hemisphere attached to the top of a tube. This simplified the integration scheme which was used to model the growth of the cell. The integration scheme was based on the Euler-forward scheme.

This paper builds on the previous work. It develops a consistent integration scheme that uses the fact that the initial and growth configurations are self-similar. Thus, the elastic meridional strain, the elastic circumferential strain as well as the growth function at the self similar configuration were determined from the initial configuration by interpolation. This allowed the calculation of the growth strain rates at the self-similar configuration resulting in an expression for the growth strains as a function of time.

The paper concludes with a comparison of the results of the above two integration schemes.

Keywords fission yeast cell, self-similarity growth, turgor pressure, plasmolysed configuration, mechanics

1. Introduction

Fission yeast cells are subjected to high turgor pressure leading to large elastic deformations.

Several models and experimental results were reported in the literature on the growth of fission yeast cells [1-8]. The cell cycle starts after cell division by instantaneous pressurization of the septum wall at the New End (NE) and continuous growth at the Old End (OE). The NE follows the OE in growth, first as a hemisphere and then into a shape similar to the OE. The cell will grow to almost double in length at which time the new septum wall will form followed by the cell division.

The cell growth models in [2,3] identified three configurations:

a) The plasmolysed configuration.
b) The growth configuration due to material deposition.
c) The elastically deformed cell configuration driven by the turgor pressure.

The growth strains were assumed to depend on the elastic strains and a growth function.

In [1], we built on the models developed in [2,3]. The growth of the old end of the fission yeast cell was modeled using the self-similarity growth principle. This was justified since it was observed that the shape of the old end as well as the width of the cell were almost constant with time. The geometry of the cell was assumed to be made of a hemisphere attached to the top of a tube. This resulted in the constancy of the meridional and circumferential strains. This simplified the integration scheme which was developed to model the growth of the cell. The integration scheme was based on the Euler-forward scheme.

This paper builds on the previous work. A consistent integration scheme was developed that takes further advantage of the fact that the initial and growth configurations are self-similar. Thus, the elastic meridional strain, the elastic circumferential strain as well as the growth function at the self similar configuration were

determined from the initial configuration by interpolation. This allows the calculation of the growth strain rates at the self-similar configuration resulting in the development of an expression of the growth strains as a function of time.

The paper concludes with a comparison of the results of the two integration schemes.

2. Constitutive Equations

The fission yeast cell is assumed to experience the following strains:

a. Meridional and circumferential elastic strains ($\varepsilon^e_s,\varepsilon^e_\theta$) that depend on the turgor pressure and the elastic material properties $\varepsilon^e=\varepsilon^e(P,E,\nu)$ where P is the turgor pressure, E the elastic modulus and ν the Poisson's ratio.

b. Meridional and circumferential growth strains governed by the evolution equations:

$$d(\varepsilon^g_s)/dt=\alpha.\phi(s).\varepsilon^e_s \quad \text{and} \quad d(\varepsilon^g_\theta)/dt=\alpha.\phi(s).\varepsilon^e_\theta \qquad (1)$$

where α is a growth factor and ϕ(s) is the growth function that depends on the meridional distance, s, measured from the tip of the OE. The value of $\phi(s)|_{s=0}$ is 1.

3. Numerical Integration Schemes

First, the geometry used was updated from a constant-zero curvature for a sphere-tube used in [1] to a continuous curvature.

Second, two schemes were considered in the numerical integration of the growth strains:

A. A forward-Euler numerical integration scheme (discussed in [1] for constant meridional and circumferential strains), and

B. A consistent numerical integration scheme.

In both cases, the upper half of a symmetrical cell was modeled. In the following, the two integration schemes will be described.

A. Forward-Euler Integration Scheme

Integrating the meridional and circumferential growth strains using the Euler-forward integration scheme for a time increment Δt from time t_m to time t_{m+1} results in:

$$(\varepsilon^g_s)_{m+1}=(\varepsilon^g_s)_m+\alpha.\phi(s).\varepsilon^e_s.\Delta t \quad \text{and} \quad (\varepsilon^g_\theta)_{m+1}=(\varepsilon^g_\theta)_m+\alpha.\phi(s).\varepsilon^e_\theta.\Delta t \qquad (2)$$

To develop the solution, the initial shape was discretized into n elements with n+1 nodes (A_1,A_{n+1}). Their corresponding locations in the self-similar configuration are designated as (a_1,a_{n+1}). Segment (a_n,a_{n+1}) becomes vertical, representing the growth of the cell. This vertical growth of the cell was assumed to be caused by the viscous growth strains.

To determine the growth function ϕ and the growth parameter α we proceed as follows: Since the radius of the cell is almost constant during growth, node A_{n+1} is assumed fixed. The time Δt and the location of node a_n are determined as shown below:

1) Calculation of time Δt

The integration scheme described in [1] was modified to include the non-constant values of meridional and circumferential strains.

When node A_n with coordinates (R_{An}, Z_{An}) moves to $a_n(R_{An+1},\text{height})$, as shown in Fig. 1, the radial motion u_r of A_n and the extension of (A_n,A_{n+1}) are given by:

$$u_r=R_{An}*\varepsilon^g_\theta(n)=R_{An}*\alpha*\phi(s_{An})*\varepsilon^e_\theta(n)*\Delta t=R_{An+1}-R_{An}=>\alpha*\phi(s_{An})=(R_{An+1}/R_{An}-1)/(\varepsilon^e_\theta(n)*\Delta t) \qquad (3)$$

and,

$$a_{n+1}a_n = A_{n+1}A_n*(1+(\varepsilon^g_s)_{av})=A_{n+1}A_n*(1+\alpha*(½)(\phi(s_{An+1})\varepsilon^e_s(n+1)+\phi(s_{An})\varepsilon^e_s(n))*\Delta t)=v*\Delta t \qquad (4)$$

where v is the velocity of tip growth of the OE.

Replacing eq. (3) into eq. (4) and noting that $\phi(s_{An+1})=0$, we get

$$A_nA_{n+1}*(1+(½)*(R_{An+1}/R_{An}-1)*(\varepsilon^e_s(n)/(\varepsilon^e_\theta(n)))=v*\Delta t \text{ or}$$

$$\Delta t=(A_nA_{n+1}/v)*(1+(½)*(R_{An+1}/R_{An}-1)*(\varepsilon^e_s(n)/(\varepsilon^e_\theta(n))) \qquad (5)$$

Similar procedure as in [1] could be followed to determine the locations of nodes a_n and a_i for i<n.

B. Consistent Numerical Integration Scheme

In the previous section, the growth strains at time "m+1" were determined using the forward-Euler integration scheme. The self-similarity principle allows the development of a consistent numerical integration scheme that uses the fact that the distribution of the strains and growth function are the same at the initial and self-similar configurations for steady state growth.

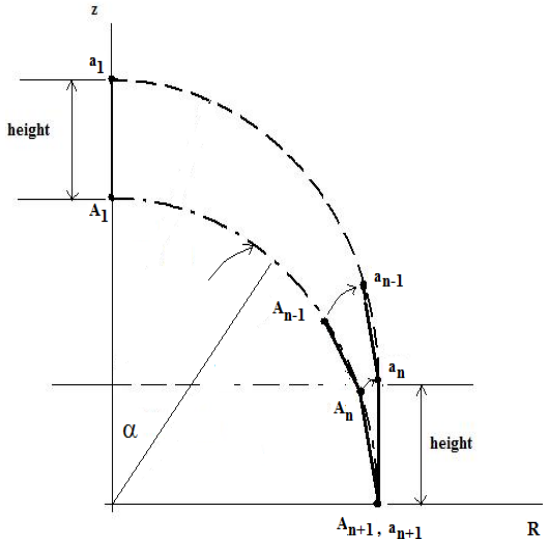

Figure 1: Self-Similarity of Growth

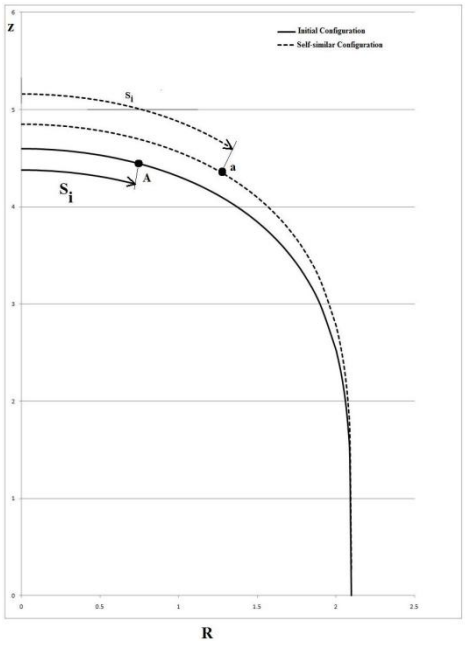

Figure 2: Meridional positions S_i and s_i at theinitial and self-similar configurations, respectively

At time t_m , for a node "A" at distance "S_i" from the tip in the meridional direction, the meridional and circumferential elastic strains (ε^e_s,ε^e_θ) due to the turgor pressure can be determined from the finite element solution.

Due to material deposition and cell growth, node "A" will move to node 'a' with the new meridional distance "s_i" from the tip, as shown in Fig. 2. For the distance "s_i", the elastic meridional and circumferential strains at time "m+1" can be determined by interpolation from the previous distribution (ε^e_s,(S), ε^e_θ(S)) since the new shape is similar to the one at time "m" with an additional vertical part that will have little effect on the strain distribution.

Mathematically, this could be expressed as follows with $t_m=0$ and $t_{m+1}=\Delta t$:

At t=0, $d\varepsilon^g_s/dt(S_i,t=0) = \alpha\phi(S_i)*\varepsilon^e_s(S_i)$ and $\varepsilon^g_s(S_i,t=0) = 0$ (updated configuration) (6)

At t=0+Δt, $d\varepsilon^g_s/dt(s_i,t=0+\Delta t)_i = \alpha\phi(s_i)*\varepsilon^e_s(s_i)$ (7)

The growth strain at time t=0+Δt can be determined by fitting a second degree polynomial to the values of ε^g_s and $d\varepsilon^g_s/dt$ at times t=0 and t=0+Δt. This gives:

$\varepsilon^g_s(s_i,t=0+\Delta t) = \varepsilon^g_s(S_i,t=0)+ d\varepsilon^g_s/dt(S_i,t=0) *t+(1/(2*\Delta t))*(d\varepsilon^g_s/dt(s_i,t=0+\Delta t) - d\varepsilon^g_s/dt(S_i,t=0))*t^2$

Using the strain and strain rates from eqs. (6) and (7) in the above equation, we get at t=0+Δt,

$\varepsilon^g_s(s_i, t=0+\Delta t)_i = (½)(\alpha\phi(S_i)*\varepsilon^e_s(S_i,t=0)_i + \alpha\phi(s_i)*\varepsilon^e_s(s_i,t=0+\Delta t)_i)*\Delta t$ (8)

$\varepsilon^g_s(s_{i+1}, t=0+\Delta t)_{i+1} = (½)(\alpha\phi(S_{i+1})*\varepsilon^e_s(S_{i+1},t=0)_{i+1} + \alpha\phi(s_{i+1})*\varepsilon^e_s(s_{i+1},t=0+\Delta t)_{i+1})*\Delta t$

In this case, the time Δt and the location of node a_n are determined as follows:

1) Determination of time Δt

When node A_n with coordinates (R_{An}, Z_{An}) moves to $a_n(R_{An+1},\text{height})$, the radial motion u_r of A_n and the extension of (A_n,A_{n+1}) are given by:

$u_r=R_{An}*\varepsilon^g_\theta(s_n)=R_{An}*(½)*\alpha*\phi(S_n)*\varepsilon^e_\theta(S_n)*\Delta t=R_{An+1}-R_A$

$=>\alpha*\phi(S_{An})=2*(R_{An+1}/R_{An}-1)/(\varepsilon^e_\theta(S_n)*\Delta t)$ (9a)

and,

$a_{n+1}a_n = A_{n+1}A_n*(1 + (½)*(\varepsilon^g_s(s_n) + \varepsilon^g_s(s_{n+1})))$

$= A_{n+1}A_n*(1 + (½)*\{(½)\alpha*\phi(S_n)\varepsilon^e_s(S_n) \}*\Delta t)=v*\Delta t$ (9b)

where v is the velocity of tip growth. Note that the values of $\alpha*\phi(S_{n+1}) =\alpha*\phi(s_{n+1}) =\alpha*\phi(s_n) =0$ were used in the above equations. Replacing eq.(9a) into eq.(9b) , we get

$A_nA_{n+1}*(1 + (½)*(R_{An+1}/R_{An} - 1)*(\varepsilon^e_s(S_n)/(\varepsilon^e_\theta(S_n)))= v*\Delta t$ or

$\Delta t =(A_nA_{n+1}/v)*(1 + (½)*(R_{An+1}/R_{An} - 1)*(\varepsilon^e_s(S_n)/(\varepsilon^e_\theta(S_n)))$ (10)

2) Location of node a_n

From the above derivations, we conclude that:

$\alpha*\phi(S_n)=2*(R_{An+1}/R_{An}-1)/(\varepsilon^e_\theta(S_n)*\Delta t)$, $R_{an} = R_{An} + R_{An}*(½)*\alpha*\phi(S_n)*\varepsilon^e_\theta(S_n)*\Delta t$ and

$z_{an} =$ height $= v*\Delta t$ (11)

3) Location of node a_i, i<n

In general, two cases need to be considered:

a. Case I: $S_i < s_i < S_{i+1}$

b. Case II: $S_{i+1} < s_i < S_{i+2}$

However, for small time increments the meridional growth length is limited and case II is seldom needed. This was the situation for the time step used in this analysis.

a. Case I: $S_i < s_i < S_{i+1}$

Assume $S_i < s_i < S_{i+1}$, then,

$\varepsilon^e_s(s_i) = \varepsilon^e_s(S_i)*(s_i-S_{i+1})/(S_i-S_{i+1}) + \varepsilon^e_s(S_{i+1})*(s_i-S_i)/(S_{i+1}-S_i)$ (12)

$\varepsilon^e_\theta(s_i) = \varepsilon^e_\theta(S_i)*(s_i-S_{i+1})/(S_i-S_{i+1}) + \varepsilon^e_\theta(S_{i+1})*(s_i-S_i)/(S_{i+1}-S_i)$

$\alpha\phi(s_i) = \alpha\phi(S_i)*(s_i-S_{i+1})/(S_i-S_{i+1}) + \alpha\phi(S_{i+1})*(s_i-S_i)/(S_{i+1}-S_i)$

For i<(n-1), $s_i = S_{total} - \Sigma^{i+2}_{j=n}(a_{j-1}a_j) - a_ia_{i+1}$ (13)

where S_{total} is the total length of the tip section that is continually reproduced ($S_{an}=S_{total}$) with

$a_ia_{i+1} = A_iA_{i+1}*\{ 1 + (½)*(\varepsilon^g_s(t=0+\Delta t)_i + \varepsilon^g_s(t=0+\Delta t)_{i+1}) \}$ (14)

Using Eqs. (8) and (14) into s_i , we get:

$s_i = S_{total} - \Sigma^{i+2}_{j=n}(a_{j-1}a_j) - A_iA_{i+1}*\{ 1 + (½)*[\varepsilon^g_s(s_i) + \varepsilon^g_s(s_{i+1})] \}$ (15)

$s_i = S_{total} -\Sigma^{i+2}_{j=n}(a_{j-1}a_j) - A_iA_{i+1}*\{1 +(½)*[(½)(\alpha\phi(S_i)*\varepsilon^e_s(S_i)+\alpha\phi(s_i)*\varepsilon^e_s(s_i))*\Delta t+\varepsilon^g_s(s_{i+1})] \}$ (16)

$s_i -S_{total} +\Sigma^{i+2}_{j=n}(a_{j-1}a_j) +A_iA_{i+1}*\{1+(½)*[\varepsilon^g_s(s_{i+1})] \}$

$$=- (¼)*A_iA_{i+1}*\Delta t*\{\alpha\phi(S_i)*\varepsilon^e_s(S_i) + \alpha\phi(s_i)*\varepsilon^e_s(s_i)\} \quad (17)$$

$$\text{Let } W_i = S_{total} - \Sigma^{i+2}_{j=n}(a_{j-1}a_j) - A_iA_{i+1}*\{ 1 + (½)*[\varepsilon^g_s(s_{i+1})] \} \quad (18)$$

then

$$s_i - W_i = - (¼)*A_iA_{i+1}*\Delta t*\{ \alpha\phi(S_i)*\varepsilon^e_s(S_i) + \alpha\phi(s_i)*\varepsilon^e_s(s_i) \} \quad (19)$$

And,

$$\{s_i - W_i\}/\{- (¼)*A_iA_{i+1}*\Delta t\} =\{ \alpha\phi(S_i)*\varepsilon^e_s(S_i) + \alpha\phi(s_i)*\varepsilon^e_s(s_i) \} \quad (20)$$

The above equations could be expanded to give:

$$\{s_i - W_i\}/\{- (¼)*A_iA_{i+1}*\Delta t\} =$$

$$\{ \alpha\phi(S_i)*\varepsilon^e_s(S_i) + [\alpha\phi(S_i)*(s_i-S_{i+1})/(S_i-S_{i+1}) + \alpha\phi(S_{i+1})*(s_i-S_i)/(S_{i+1}-S_i)]*\varepsilon^e_s(s_i) \} \quad (21)$$

After some simplifications, one gets:

$$\alpha\phi(S_i)=[\{s_i-W_i\}/\{-(¼)*A_iA_{i+1}*\Delta t\}$$
$$-\alpha\phi(S_{i+1})*\varepsilon^e_s(s_i)*(s_i-S_i)/(S_{i+1}-S_i)]/[\varepsilon^e_s(S_i)+\varepsilon^e_s(s_i)*(s_i-S_{i+1})/(S_i-S_{i+1})] \quad (22)$$

For a given s_i, we can calculate $\alpha\phi(S_i)$. If node "i" is on the self-similar configuration, the solution is reached. Otherwise, the nonlinear iteration scheme on s_i is continued until compatibility is satisfied.

4. Simulation Results

For the Euler-forward numerical integration scheme, the resulting distributions of $d(\varepsilon^g_s)/dt$ and $d(\varepsilon^g_\theta)/dt$ are shown in Fig. 3. These plots matches better the results of [2]. For the consistent numerical integration scheme, the distributions of $d(\varepsilon^g_s)/dt$ and $d(\varepsilon^g_\theta)/dt$ at S_i and s_i are shown in Fig. 4.

The growth functions $\alpha\phi$, for both the Euler-forward and Consistent integration schemes, are plotted in Fig. 5. For small time steps, the two schemes are close with a relative error w.r.t. $\alpha\phi(1)$ less than 3%.

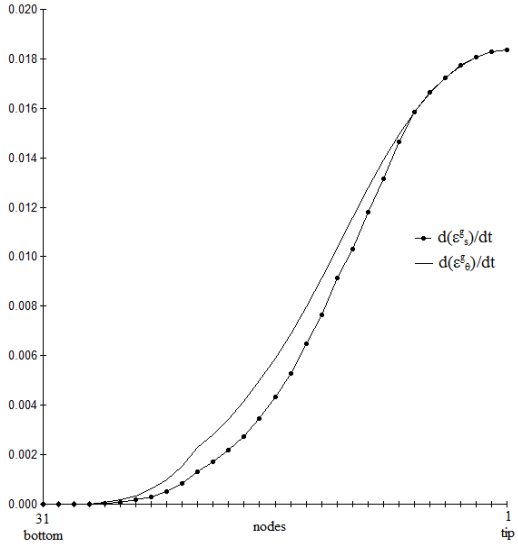

Figure 3: $d(\varepsilon^g_s)/dt$ and $d(\varepsilon^g_\theta)/dt$ versus node number, Euler-forward scheme (min^{-1}).

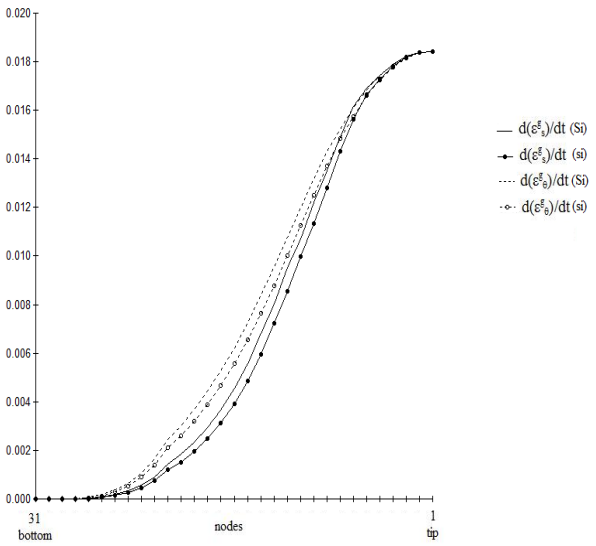

Figure 4: $d(\varepsilon^g_s)/dt$ and $d(\varepsilon^g_\theta)/dt$ versus node number at S_i and s_i using consistent integration scheme (min^{-1}) .

5. Conclusions

In a previous publication, a simplified method to model the growth of a fission yeast cell using the self-similarity principle was introduced. In this case, the old end of the yeast cell was modeled as an independent hemisphere on the top of a tube. This resulted in the meridional and circumferential elastic strains being constant in the hemisphere, thus simplifying the approach to finding the growth function. An improvement on the previous modeling took further advantage of the similarity of the initial and growth configurations resulting in a consistent numerical integration scheme. The elastic meridional strain, the elastic circumferential strain as well as the growth function at the self similar configuration were determined from the initial configuration by

interpolation. This allowed the calculation of the growth strain rates at the self-similar configuration resulting in an expression for the growth strains as a function of time.

For small time steps, the growth function as well as the rate of the meridional and circumferential growth strains from the Euler-forward and consistent integration schemes were close.

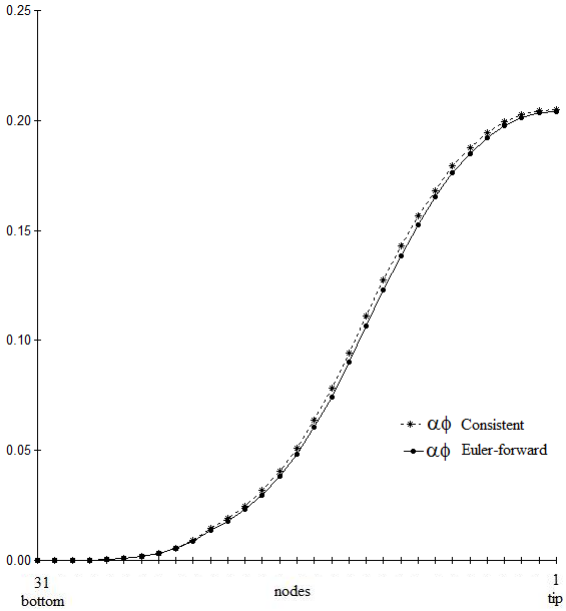

Figure 5: $\alpha\phi$ for Euler-forward and Consistent integration schemes (min^{-1})

References

[1]. Kasti, N., (2019). "Modeling the Growth of a Fission Yeast Cell Using the Self-Similarity Growth Principle - A Simplified Approach", Journal of Multidisciplinary Engineering Science and Technology, vol. 6, Issue 3.

[2]. Abenza, J., et al., (2015). "Wall Mechanics and Exocytosis Define the Shape of Growth Domains in Fission Yeast", Nature Communications, 6:8400, doi: 10.1038/ncomms9400.

[3]. Drake, T., Vavylonis, D., (2013). "Model of Fission Yeast Cell Shape Driven by Membrane Bound Growth Factors and the Cytoskeleton", PLOS Computational Biology, Vol. 9, Issue 10.

[4]. Mitchison, J., Nurse, P., (1985). "Growth in Cell Length in the Fission Yeast Schizosaccharomyces Pombe", J. Cell Sci., 75, 357-376.

[5]. Bernal, R., et al., (2007). "The Mechanics of Tip Growth Morphogenesis: what we have learned from Rubber Ballons", Journal of Mechanics of Materials and Structures, Vol. 2, No. 6.

[6]. Atilgan, E., et al., (2015). "Morphogenesis of the fission yeast cell through cell wall expansion", Current Biology, 25(16): 2150-2157.

[7]. Campas, O., Mahadevan, L., (2009). "Shape and Dynamics of tip-Growing Cells", Current Biology, 19, 2102-2107.

[8]. Goriely, O., Tabor, M., (2003). "Self-similar Tip Growth in Filamentary Organisms", The American Physical Society, Physical Review Letters, Vol. 90, No. 10.